

AD _____

(Leave blank)

Award Number: W81XWH-09-1-0021

TITLE: Improving cancer detection and dose efficiency in
dedicated breast cancer CT

PRINCIPAL INVESTIGATOR: Bian, Junguo

CONTRACTING ORGANIZATION: The University of Chicago
Chicago, IL 60637

REPORT DATE: February 2010

TYPE OF REPORT: annual summary

PREPARED FOR: U.S. Army Medical Research and Materiel Command
Fort Detrick, Maryland 21702-5012

DISTRIBUTION STATEMENT: (Check one)

☒ Approved for public release; distribution unlimited

☐ Distribution limited to U.S. Government agencies only;
report contains proprietary information

The views, opinions and/or findings contained in this report are those of the author(s) and should not be construed as an official Department of the Army position, policy or decision unless so designated by other documentation.

REPORT DOCUMENTATION PAGE				<i>Form Approved OMB No. 0704-0188</i>	
<small>The public reporting burden for this collection of information is estimated to average 1 hour per response, including the time for reviewing instructions, searching existing data sources, gathering and maintaining the data needed, and completing and reviewing the collection of information. Send comments regarding this burden estimate or any other aspect of this collection of information, including suggestions for reducing the burden, to Department of Defense, Washington Headquarters Services, Directorate for Information Operations and Reports (0704-0188), 1215 Jefferson Davis Highway, Suite 1204, Arlington, VA 22202-4302. Respondents should be aware that notwithstanding any other provision of law, no person shall be subject to any penalty for failing to comply with a collection of information if it does not display a currently valid OMB control number.</small> PLEASE DO NOT RETURN YOUR FORM TO THE ABOVE ADDRESS.					
1. REPORT DATE (DD-MM-YYYY) 25/02/2010		2. REPORT TYPE Annual summary		3. DATES COVERED (From - To) 26 Jan 2009 – 25 Jan 2010	
4. TITLE AND SUBTITLE Improving cancer detection and dose efficiency in dedicated breast cancer CT				5a. CONTRACT NUMBER W81XWH-09-1-0021	
				5b. GRANT NUMBER BC083239	
				5c. PROGRAM ELEMENT NUMBER	
6. AUTHOR(S) Bian, Junguo Email: junguo@uchicago.edu				5d. PROJECT NUMBER	
				5e. TASK NUMBER	
				5f. WORK UNIT NUMBER	
7. PERFORMING ORGANIZATION NAME(S) AND ADDRESS(ES) University of Chicago Department of Radiology, 5841 South Maryland Ave., MC2026 Chicago, IL 60637				8. PERFORMING ORGANIZATION REPORT NUMBER	
9. SPONSORING/MONITORING AGENCY NAME(S) AND ADDRESS(ES) U.S. Army Medical Research and Materiel Command Fort Detrick, Maryland 21702-5012				10. SPONSOR/MONITOR'S ACRONYM(S)	
				11. SPONSOR/MONITOR'S REPORT NUMBER(S)	
12. DISTRIBUTION/AVAILABILITY STATEMENT Approved for public release; distribution unlimited					
13. SUPPLEMENTARY NOTES					
14. ABSTRACT Breast cancer is the second leading cause of cancer mortality among women in America. Dedicated breast computed tomography (CT) has been developed for potential use as an imaging tool for breast-cancer screening or diagnosis, because it can yield three-dimensional (3D) volumetric images of the breast, thus overcoming inherent limitations of conventional two-dimensional (2D) mammography. Image quality and the radiation dose are of important concerns in breast CT imaging. The objective of this project is to investigate and develop innovative imaging configurations and reconstruction algorithms for obtaining accurate images and reducing radiation dose in breast CT imaging. In the past year, I have studied and assessed several non-circular configurations that could be potentially useful for breast CT imaging by investigating data conditioning techniques and reconstructing images for the configurations. I have also conducted preliminary studies using innovative optimization-based algorithms for a potentially substantial reduction of radiation dose in breast CT imaging. In addition to computer-simulation studies, I have also performed real data studies involving physical phantoms and patient data. In summary, during the first year, I have successfully carried out research on the					
15. SUBJECT TERMS Breast CT, image reconstruction, imaging configuration, total variation minimization					
16. SECURITY CLASSIFICATION OF:			17. LIMITATION OF ABSTRACT UU	18. NUMBER OF PAGES 22	19a. NAME OF RESPONSIBLE PERSON USAMRMC
a. REPORT U	b. ABSTRACT U	c. THIS PAGE U			19b. TELEPHONE NUMBER (Include area code)

Table of Contents

	<u>Page</u>
Introduction.....	4
Body.....	5
Key Research Accomplishments.....	10
Reportable Outcomes.....	11
Conclusion.....	12
References.....	13
Appendices.....	14

INTRODUCTION

Breast cancer is the most frequently diagnosed cancer and the second leading cause of cancer mortality among women in America [1]. Researchers are actively developing breast imaging techniques, including breast tomosynthesis [2] and dedicated breast computer tomography CT [3,4], that can form three-dimensional (3D) images of the breast, thus potentially overcoming inherent limitations of conventional two-dimensional (2D) mammography. Several prototypes of dedicated breast CT scanners have been built in different institutions throughout US. Current scanners employ a circular imaging configuration for data collection and the FDK algorithm for approximate image reconstruction. However, it is well-known that a circular imaging configuration does not yield sufficient data for mathematically exact image reconstruction. Also, because the FDK algorithm requires data collected at a large number of projection views, and because the total dose in breast CT imaging is typically about the same as that in a two-view mammography, the number of photons collected at each view can be severely limited. As such, the projection data at each view have very low signal-to-noise ratio (SNR), thus severely limiting the breast-CT-image quality.

Clearly, image quality and radiation dose are great concerns in breast CT imaging. The objective of this research is to investigate and develop innovative imaging configurations and reconstruction algorithms for obtaining accurate images and reducing radiation dose in breast CT imaging. In the past year, my efforts for the project have been supported by a Predoctoral Traineeship Award, and I have performed research tasks as planned. As discussed below, I have studied and assessed several potentially useful non-circular configurations for breast CT imaging by investigating data conditioning techniques and reconstructing images for the configurations. I have also conducted preliminary studies using innovative optimization-based algorithms for a potentially substantial reduction of radiation dose in breast CT imaging. In addition to computer-simulation studies, I have performed real data studies involving physical phantoms and patients provided by the collaborators. In summary, during the first year, I have successfully carried out research on the tasks planned, and the results obtained have formed a solid basis for me to continue the research planned for the next year.

BODY

1 Training Accomplishments

At the time of this report, as the recipient of the Predoctoral Traineeship Award, I have taken 20 out of 20 required courses towards my Ph.D. degree in Medical Physics. The courses include physics of medical imaging, physics of radiation therapy, mathematics for medical physicists, statistics, anatomy of the body, radiation biology, and teaching assistant training.

2 Research Accomplishments

2.1 Investigation of non-circular imaging configurations

Current prototype breast CT scanners employ a circular scanning configuration for data acquisition and the FDK algorithm for approximate image reconstruction. The circular scanning configuration is easy to implement and can provide an efficient coverage of the breast when a flat-panel detector is used. The FDK algorithm, although it is a mathematically approximate algorithm, remains the widely used algorithm for commercial scanners because of its easy implementation and computational efficiency. However, the circular imaging configuration yield data that are insufficient for mathematically exact reconstruction of a three-dimensional (3D) breast. For example, in an FDK reconstruction, images within two-dimensional (2D) slices away from the source plane suffer from artifacts such as contrast reduction and streaks, which can lead to an increased false positive and/or false negative diagnosis. In order to acquire data sufficient for accurate 3D reconstruction, non-circular scanning configurations have been proposed and investigated. In the first-year research, I have investigated a number of imaging configurations, as described below, that can yield data sufficient for mathematically exact image reconstruction of the breast.

Helical imaging configuration: The helical imaging configuration is a natural extension of the circular imaging configuration and it can yield data sufficient for accurate 3D reconstruction of the breast. In a helical configuration, the X-ray source and detector are translated while they are rotating, and the source trajectory can be expressed as

$$\vec{r}_0(\lambda) = \left(R \cos \lambda, R \sin \lambda, \frac{h}{2\pi} \lambda \right)^T, \quad (1)$$

where λ is the view angle, R the distance from the source point to the rotation axis, and h the pitch of the helical trajectory, which is defined as the translation distance during one turn of rotation. I have investigated the helical configuration using both simulated and real data. The imaging configuration of our simulation study is identical to that of the prototype scanner at the University of California, Davis. In the configuration, which has been used to acquire real data of physical phantom and patient breast, the distances of the source to the detector plane and to the center of rotation are 87.78 cm and 45.83 cm. The size of the flat-panel detector is 39.7×29.7 cm² consisting of 1024×768 detector channels. In the simulation study, I have used different digital phantoms, such as the Defrise disk phantom, to generate data at 500 views using analytic projection equations of the phantoms for every turn with helical pitches ranging from 3 cm to 11 cm. I used the disk phantom in the simulation study because it is a challenging phantom that has been used widely for evaluation of image reconstruction algorithms. I investigated the volume

coverage that can be reconstructed exactly using different helical pitches. The simulation study results show that smaller pitch needs more turns to cover the same volume and will thus result in elevated radiation dose to the patient (assuming dose per view is fixed). However, a smaller pitch can result in better coverage for the volume than larger helical pitch.

I have also investigated and evaluated the helical configurations on the prototype scanner. From a physical Defrise disk phantom and a sacrificed mouse, data were collected by use of four different helical pitches ranging from 6 cm to 10 cm. The data acquired from the prototype system requires several steps of processing so that they can be used for image reconstruction. Data processing was carried out for removal of data artifacts, including detector-response correction, reference projection estimation, and physical factor correction. The detector-response correction compensates for the non-uniform response of detector channels and removes dead/defect detector channels if correction is not possible. The reference projection is a projection acquired in the absence of the imaged object and is required for the conversion of the raw measurements to data for image reconstruction. I created the data for image reconstruction by taking the logarithm of the ratio between reference projection and object projections. I have estimated the reference projection by choosing the average of pixel values over a region unattenuated by the object and using the value as a uniform reference projection. The assumptions behind this are that the detector response is uniform and that the object is sufficiently small so that its projection will not fully cover the detector. I have also compared the volume coverage in real data studies for different helical pitches. In order to cover the breast volume of a patient, it may require small pitch with multiple turns because of its better volume coverage, thus radiation dose can be a concern for such helical configurations. In order to reduce radiation dose, the dose at each view for a helical configuration need to be reduced. Given the fact that the dose level per view is already low and that the projection data have significant quantum noise, it seems unrealistic to further reduce the dose for each view in a helical configuration.

Saddle imaging configuration: Saddle imaging configuration is another configuration that can generate data sufficient for exact 3D reconstruction of the breast. The saddle configuration can be interpreted as a generalization of the circular configuration, in which the z-component of the X-ray source will vary periodically. The saddle trajectory under study can be expressed as

$$\vec{r}_0(\lambda) = (R \cos \lambda, R \sin \lambda, h \cos 2\lambda)^T. \quad (2)$$

I have studied the saddle imaging configurations using both simulation and real data. The geometric parameters of the simulation system is the same as what was used in the helical imaging configurations except for that different values of h were used. Again, I have used the Defrise disk phantom to generate projection data at 500 view over 2π using saddle imaging configurations. I also added Gaussian random noise terms to the source positions in order to simulate mechanical inaccuracy of the real system. I have compared projection data and reconstructed images for different saddle imaging configurations.

I then investigated the saddle imaging configuration on the prototype breast CT scanner. The implementation of a saddle configuration on the real system requires the X-ray source movement along the z-axis according to a non-linear function of the rotation angle. Because of mechanical limitations of motor control, such a non-linear movement can not be implemented directly and has to be realized through a series of analytically pre-determined source positions. Additional source positions can be interpolated between two adjacent pre-determined source positions. I have computed 100 and 250 source positions distributed equally over 2π using an analytic formula of the trajectory. Based on these pre-calculated source positions, I interpolated additional 400 or 250 source positions for additional data collection. These source positions were used for the control of the motor and data have been collected from a Defrise disk phantom and a sacrificed

mouse. I also performed detector response correction and reference image conversion on the projection data, and have investigated the volume coverage of saddle configurations. The results of the studies indicate that a saddle configuration may have a good coverage for the plane at $z = 0$, which is $\frac{h}{2}$ away from the chest wall.

Circle-plus-line imaging configuration: The circle-plus-line imaging configuration is another configuration that can yield data sufficient for exact 3D reconstruction of the breast. It can be realized by a linear scan after a circular scan, and it can be readily implemented on the current prototype scanners. I have studied this imaging configuration using simulation data. In order to cover the breast, the length for the line scan can be up to 20 cm. The configuration requires the full coverage of the breast for each view, including the linear part. Thus requiring large detector size. I generated data at 500 views for the circular scan and 500 views for the line scan from the digital Defrise disk phantom, and compared its volume coverage to that of the helical imaging configuration and saddle configuration. Our collaborators have also implemented the circle-plus-line imaging configuration on the prototype scanner, in which the Defrise disk phantom was scanned at 500 views. I have performed detector response correction and reference image conversion on the projection data.

Development of targeted region-of-interest imaging approach: I have conducted a preliminary investigation on dynamic collimation to achieve targeted ROI imaging using simulation studies [5], in which the source and the detector are moved for each view, so that after collimation, the ROI can always be covered by the beam. This imaging approach leads to an imaging problem with a relatively complex source trajectory and data truncation, which can however be solved with the back-projection filtration (BPF) algorithm [6,7]. I have used the BPF algorithm to reconstruct ROI images from truncated data collected with this imaging configuration.

2.2 Investigation and development of novel algorithms tailored to accurate reconstruction of breast CT images

Data sufficiency condition for breast CT: In breast CT, a half-cone geometry is used for reducing the radiation dose to the patient torso. This can significantly alter the data sufficiency condition for image reconstruction of the breast. I have studied the data sufficiency conditions using helical and other imaging configurations for both full-cone and half-cone geometries. For the study of half-cone geometry, I first generated simulation data with different helical pitches from the Defrise disk phantom and compared the reconstruction volume for different imaging configurations. When the source is close to the chest wall, I removed the part of the projection data that will be blocked by the patient body. This reduces the volume that can be reconstructed, especially the part near the chest wall. The study results suggest that the use of a helical imaging configuration with a half-cone geometry make it difficult to acquire data for reconstructing exactly the region near the chest wall of the patient.

Noise studies of image reconstruction: In breast CT imaging, because of the radiation concern, the total permissible radiation dose should not exceed that of a conventional mammographic examination. This can, however, result in data with a low signal-to-noise ratio (SNR) when projection data are acquired at a large number of views. In addition to statistical noise due to low dose, noise is also introduced in the signal amplification process and detector electronics, which can significantly impact the breast CT image quality. In order to study the effect of noise, I have generated noisy projection data for different imaging configurations, with different levels of Gaussian noise varying from 0.5% to 5% to represent high to low radiation dose levels. I have investigated noise properties in images reconstructed by use of FDK and BPF algorithms at different noise levels .

2.3 Investigation and development of total-variation-based algorithms for breast CT image reconstruction

Radiation dose in breast CT imaging is an important concern. Further dose reduction in breast CT can be achieved through collecting data at a reduced number of projection views. When analytic algorithms such as the FDK and BPF algorithms are applied to sparse-view data, the reconstruction images will contain artifacts such as streak artifacts that can lower significantly the image utility. Recently, algorithms based upon the minimization of image total variation (TV) subject to data condition have been developed for image reconstruction from sparse-view data [8,9]. I have conducted a preliminary study in which TV algorithms have been exploited for image reconstruction from sparse-view data in breast CT.

Data calibration and processing: In the case of sparse-view data, data information available to image reconstruction is limited, and thus it is critically important to make sure that data information is used correctly. The first issue is to make sure that data geometry is calibrated appropriately. A calibration method has been developed to obtain data geometric parameters from multiple projections of metal ball-bearing (BB) objects. Assuming that the system has a mechanically stable rotation center and that the detector is generally within the rotation plane, one can derive the geometrical relationship between the orbital paths of the individual balls for determining data geometric parameters. The calibration process consists of identifying the center position of BBs projection at each view, determining the ball orbits, and relating them to the system geometry parameters. I have further refined and validated the calibration parameters using programs for data consistency check and image reconstruction. Under certain conditions, the programs can determine the projection of the source on the detector plane to be within the size of a detector channel.

TV-based image reconstruction: Using the real patient breast data obtained from our collaborators at the University of California at Davis, I have performed a preliminary investigation of image reconstruction from sparse-view data in breast CT [10] (Appendix B). In the study, I have added projections generated from small spheres that simulate micro-calcification clusters (MCCs) to the patient data. The contrast levels of the simulated MCC structures are about 0.5 to 1 times of that of the background glandular tissues. Furthermore, I have investigated noise properties in images by reconstructing them from data on individual detector rows or from data averaged over a number of detector rows. In the latter case, the noise level in projection data is effectively reduced. The patient data sets contain projections collected at 500 views uniformly distributed over 2π . In the sparse-view data study, I first formed sparse-data sets by extracting from 500-view patient data set at 25 and 50 views uniformly distributed over 2π . I then used both TV and FDK algorithms to reconstruct images from the extracted sparse-view data sets. The reconstruction results indicate that the TV algorithm can yield generally higher contrast levels of the MCC structures than does the FDK algorithm. This conclusion applies to both data with and without averaging as discussed above. An implication of the study is that the TV algorithm can be employed for potentially reducing substantially the total radiation dose in breast CT.

2.4 Evaluation of the proposed configurations and algorithms

The evaluation study is planned largely for years 2 and 3. However, I have carried out preliminary studies on data and image noise properties this year to lay out the basis for the planned evaluation studies in the next year.

Digital breast phantom: One of the important tools in evaluation studies is the availability of digital breast phantoms containing structures with different levels of complexity. I have created

and modified two breast phantoms that consist of a half-ellipsoid object wrapped by simulated skin. The half-ellipsoid contains a compound of adipose and glandular tissue, which is also approximated by ellipsoids of different sizes. Spheres with strong attenuation (i.e., high contrast) of different sizes that mimic MCCs have also been included in the phantoms. Specifically, in a typical MCC, the smallest calcification is about 200 μm , and a MCC typically includes 3 to 10 simulated micro-calcifications. The MCCs have been added to the glandular tissues and the axillary tail of the breast. From the digital breast phantoms, I have generated projection data at 500 views uniformly distributed over 2π using a circular imaging configuration that is currently used by our collaborators. I have also generated noisy data by adding Gaussian noise to the simulated data. The digital breast phantoms and simulation tools developed provide a solid basis for the evaluation study planned for the next year.

Noise study of ROI-imaging approach: I have studied the noise properties in images reconstructed by use of the BPF algorithm in a simulation study, in which a uniform cylinder phantom is used to generate 1000 noisy data sets containing Gaussian noise. From the 1000 noisy data sets, I first reconstructed noisy images using the BPF algorithm and then computed empirical image variances and covariances. The results show that the noise level within an ROI is non-uniform and that the image noise level in the center-of-rotation region is generally lower than that in other regions. Therefore, it is important to design an imaging configuration such that the ROI can be placed near the center of rotation.

KEY RESEARCH ACCOMPLISHMENTS

- I have investigated and evaluated helical, saddle, and circle-plus-line imaging configurations for potential use in breast CT.
- I have carried out a preliminary investigation on dynamic collimation for ROI imaging using simulation data.
- I have modified and developed a BPF algorithm for image reconstruction from data acquired with non-circular imaging configurations in breast CT.
- I have modified and developed a BPF algorithm for image reconstruction from simulation data acquired in an imaging configuration employing dynamic collimation.
- In working with the collaborators, projection data of physical phantoms have been collected.
- In working with the collaborators, projection data of patient breasts have been collected.
- I have performed a preliminary investigation on potential dose reduction by lowering the number of projection views in breast CT.
- I have created digital breast phantoms with different structures and micro-calcification clusters, which can be used for quantitative evaluation of imaging configurations and reconstruction algorithms.

REPORTABLE OUTCOMES

Peer-reviewed Journal Articles

1. **J. Bian**, D. Xia, E. Y. Sidky, X. Pan: "Region of interest imaging for a general trajectory with the rebinned BPF algorithm", Tsinghua Science and Technology, Vol 15, pp 68-73, 2010.
2. **J. Bian**, X. Han, E. Y. Sidky, G. Cao, J. Lu, O. Zhou, X. Pan: "Investigation of sparse data mouse imaging using micro-CT with a carbon-nanotube-based X-ray source", Tsinghua Science and Technology, Vol 15, pp 74-78, 2010.

Conference Proceeding Articles

1. **J. Bian**, X. Han, E. Y. Sidky, G. Cao, J. Lu, O. Zhou, X. Pan: "Investigation of sparse-data mouse imaging using micro-CT with a carbon-nanotube X-ray source", Proceeding of 10th International Meeting on Fully Three-Dimensional Image Reconstruction in Radiology and Nuclear Medicine, Beijing, China, 2009
2. **J. Bian**, X. Han, E. Y. Sidky, D. Tward, J. H. Siewerdsen, X. Pan: "Sparse data reconstruction of flat-panel cone-beam CT for potential use in Image-guided surgery", Proceeding of 10th International Meeting on Fully Three-Dimensional Image Reconstruction in Radiology and Nuclear Medicine, Beijing, China, 2009

Conference Presentations and Abstracts

1. **J. Bian**, X. Han, K. Yang, N. Packard, E. Sidky, J. Boone, X. Pan: "A feasibility study of breast CT imaging with substantially lowered radiation dose", 2009 IEEE Nuclear Science Symposium and Medical Imaging Conference, Orlando, FL, Oct-2009

CONCLUSIONS

As the recipient of the Predoctoral Traineeship Award, I have finished the required courses towards my Ph.D. degree. These trainings have proven useful for me to achieve the proposed research goals.

During the first year, I have investigated and evaluated non-circular imaging configurations potentially useful for breast CT imaging by studying data sufficiency conditions and by performing both simulation and real data studies. I have developed and modified BPF algorithms to reconstruct images within an ROI from data containing truncations. The modified BPF algorithm can yield more accurate images than the existing FDK algorithm. In an attempt to further reduce imaging dose, one may reduce the number of views at which projection data are collected. In this situation, analytic algorithms may not provide adequate results. Instead, I have developed, modified, and implemented the TV algorithm to reconstruct images from sparse-view data. Also, I have created digital breast phantoms that can be used as an important tool for evaluation of the potential utility of imaging configurations and reconstruction algorithms. Furthermore, I have performed a preliminary evaluation study of different reconstruction algorithms in which both simulation and real data were used.

In summary, I believe that I have achieved the goals planned for the first year and laid down the foundation for the research in the next two years. The aims in the next two years include further development of the TV algorithm for image reconstruction in low-dose breast CT, investigation of the effects of physical factors on the quality of image reconstruction, and performance of well designed evaluation studies.

REFERENCES

1. Cancer Fact and Figures, American Cancer Society, 2009 (<http://www.cancer.org/downloads/STT/500809web.pdf>)
2. J. T. Dobbins III and D. J. Godfrey: "Digital X-ray tomosynthesis: current state of the TV and clinical potential", *Phys. Med. Biol.*, Vol. 48, pp. R65-R106, 2003. A
3. J. M. Boone, A. L. Kwan, K. Yang, G. W. Burkett, K. K. Lindfors and T. R. Nelson: "Computed tomography for imaging the breast", *J. Mammary Gland Biol. Neoplasia*, Vol.11, pp103-111, 2006.
4. Chen B and Ning R: "Cone-beam volume CT breast imaging: Feasibility study", *Med. Phys.*, 29:755-770, 2002. Vol. 6913, 69134G, 2008
5. J. Bian, H. Zhang, P. Zhang, and X. Pan: "A cone-beam Approach of ROI Imaging with a Detector Smaller than the Imaged Object", *Proceeding of 9th International Meeting on Fully Three-Dimensional Image Reconstruction in Radiology and Nuclear Medicine*, pp. 386-389, 2007
6. Y. Zou, and X. Pan: "Exact image reconstruction on PI-line from minimum data in helical cone-beam CT", *Phys. Med. Biol.*, 49: 941-959, 2004.
7. Y. Zou, and X. Pan, and E. Y. Sidky: "Theory and algorithms for image reconstruction on chords and within regions of interest", *J. Opt. Soc. Am.*, A22: 2372-2384, 2005.
8. E. Y. Sidky, C.-M. Kao, and X. Pan: "Accurate image reconstruction from few-views and limited-angle data in divergent-beam CT", *J. X-ray Sci. Tech.*, Vol. 14, pp. 119-139, 2006.
9. E. Y. Sidky and X. Pan: "Image reconstruction in circular cone-beam computed tomography by constrained, total-variation minimization", *Phys. Med. and Bio.*, Vol. 53, pp. 4777-4807, 2008.
10. J. Bian, X. Han, K. Yang, N. Packard, E. Sidky, J. Boone, X. Pan: "A feasibility study of breast CT imaging with substantially lowered radiation dose", 2009 IEEE Nuclear Science Symposium and Medical Imaging Conference, Orlando, FL, Oct-2009

APPENDICES

- Appendix A: **J. Bian**, D. Xia, E. Y. Sidky, X. Pan: "Region of interest imaging for a general trajectory with the rebinned BPF algorithm", Tsinghua Science and Technology, Vol 15, pp 68-73, 2010.
- Appendix B: **J. Bian**, X. Han, K. Yang, N. Packard, E. Sidky, J. Boone, X. Pan: "A feasibility study of breast CT imaging with substantially lowered radiation dose", 2009 IEEE Nuclear Science Symposium and Medical Imaging Conference, Orlando, FL, Oct-2009

Region of Interest Imaging for a General Trajectory with the Rebinned BPF Algorithm^{*}

BIAN Junguo^{**}, XIA Dan, SIDKY Emil Y, PAN Xiaochuan

Department of Radiology, University of Chicago, 5841 S. Maryland Avenue, Chicago, IL 60637, USA

Abstract: The back-projection-filtration (BPF) algorithm has been applied to image reconstruction for cone-beam configurations with general source trajectories. The BPF algorithm can reconstruct 3-D region-of-interest (ROI) images from data containing truncations. However, like many other existing algorithms for cone-beam configurations, the BPF algorithm involves a back-projection with a spatially varying weighting factor, which can result in the non-uniform noise levels in reconstructed images and increased computation time. In this work, we propose a BPF algorithm to eliminate the spatially varying weighting factor by using a rebinned geometry for a general scanning trajectory. This proposed BPF algorithm has an improved noise property, while retaining the advantages of the original BPF algorithm such as minimum data requirement.

Key words: computed tomography; region of interest; general trajectory; rebinned backprojection-filtration

Introduction

Significant advances have been made in the development of theoretically exact algorithms for image reconstruction from cone-beam projections. Theoretically exact algorithms that were developed initially for a helical trajectory^[1-3] have been extended to reconstruct images from cone-beam projections acquired with general source trajectories^[4-8]. The back-projection-filtration (BPF) algorithm is one of the recently developed algorithms^[9-11]. It can be applied to reconstructing images for a wide class of general scanning trajectories and is capable of reconstructing an image within a region-of-interest (ROI) from projection data containing truncations. This property of the BPF algorithm

allows imaging applications of practical significance. For example, in non-conventional computed tomography (CT) applications, it is not uncommon that the available detector covers only a portion of a field of view (FOV) that is needed otherwise for completely covering the entire support of the imaged object. Moreover, data acquisition in many practical applications is achieved through the rotation of the object around the physical center of rotation, which is often chosen as the center of mass of the object and may be at a distance from the FOV center, as shown in Fig. 1. Although this imaging approach leads to an imaging problem with a relatively complex source trajectory and data truncation, one can apply the BPF algorithm to reconstructing an ROI image from truncated data collected with this kind of imaging configurations with general trajectories^[12].

Like many existing algorithms for divergent-beam configurations, the original BPF algorithm also involves the computation of a spatially varying weighting factor in its back-projection step, which can result in non-uniform noise levels in reconstructed images and increased computation time^[13-16]. Therefore, it is desirable to eliminate the spatially varying weighting

Received: 2009-10-25

^{*} Supported in part by National Institutes of Health (Nos. EB000225 and CA120540). J. Bian was supported by the DoD Predoctoral Training Grant (No. BC083239), and E. Y. Sidky was supported in part by the Career Development Award from NIH SPORE (No. CA125183-03).

^{**} To whom correspondence should be addressed.

E-mail: junguo@uchicago.edu

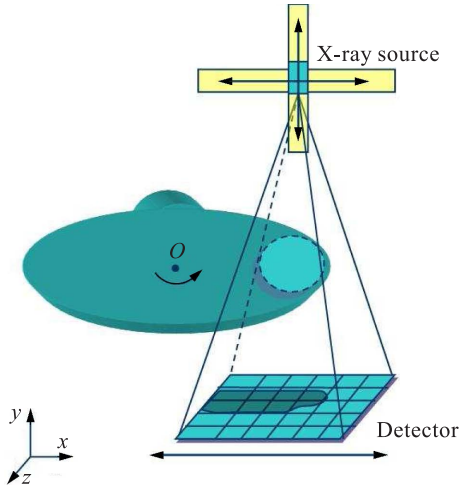


Fig. 1 Illustration of the 3-D imaging configuration. The object rotates around the rotation axis O . The source can move freely vertically and horizontally while the detector can only move horizontally. The region enclosed by the dashed curve indicates the FOV covered by the detector.

factor in the BPF algorithm for improving its noise properties and computational efficiency. In this work, based upon the original BPF algorithm, we propose a BPF algorithm in terms of a rebinned geometry for a general scanning trajectory designed for ROI imaging, in which no spatially varying weighting factor is involved in the back-projection step. The use of the rebinned geometry can not only eliminate the spatially varying weighting factor, thus improving the noise properties of BPF reconstructions, but also retain the properties of the original BPF algorithm such as minimum data requirement and ROI-image reconstruction from truncated data.

1 New ROI Imaging Approach

1.1 Design of an ROI imaging approach

We display in Fig.1 a 3-dimensional (3-D) scanning configuration under consideration, in which the object rotates around the rotation axis, the source can move freely vertically and horizontally, and the detector can only move horizontally. The line connecting the source and the detector center is always perpendicular to the detector plane. A sketch of this scanning geometry within 2-dimensional (2-D) slice at $z=0$ is shown in Fig. 2. An ellipsoid support enclosed by the thin curve represents the imaged object in which an ROI is indicated as the shaded region, and the FOV is

enclosed by a thick curve. The geometric center of the ellipsoid is placed at the physical center of rotation of the imaging system, which is also chosen as the origin of the fixed coordinate system. We assume that the distance of the FOV center to the physical center of rotation is R_0 , that the width of the detector is $2D$, and that the distance H between the physical center of rotation and the detector remains constant. Let R denote the radius of the FOV. Clearly, $R < D$ for the cone-beam projection under consideration. Projections at different views are collected through the rotation of the object about the physical rotation center and the motion of the source and detector in the space, which is constrained by two conditions: (1) the size of the FOV (enclosed by the thick curve) formed by the source and detector remains unchanged and always covers the ROI, and (2) the source point, the FOV center, and the detector mid-point always remain on the same line, which, without loss of generality, is assumed to be perpendicular to the detector plane. An additional constraint on the source is that it is outside the rotating object.

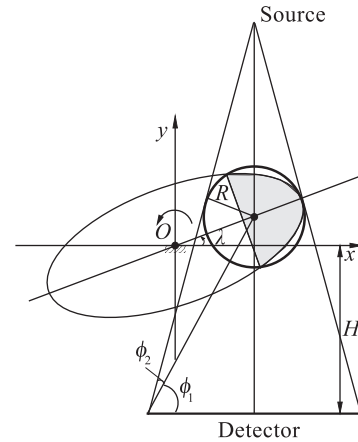


Fig. 2 Illustration of the scanning geometry within 2-D slice at $z=0$. The support of the imaged object is enclosed by the thin curve. During imaging, the object rotates around the physical center of rotation. The ROI (shaded area) to be imaged is within the FOV (enclosed by the thick curve) formed by the source and the detector. When the object is rotated, the detector can move only along x -axis, whereas the source can move along x - and/or y -axes so that the FOV always covers the ROI completely.

1.2 Source trajectory

When the imaged object rotates, the source and the detector are moved accordingly so that they form an

FOV that always covers the ROI. Consequently, the location of the FOV center also changes. Considering the motion constraints on the source and detector described above, one can determine the trajectories of the source, the FOV center, and the mid-point of the detector in the x - y plane. Let λ denote the rotation angle of the object, which is defined as the angle between the long axis of the ellipsoid object and the x axis. Therefore, the trajectories of the FOV center (x_F, y_F, z_F) and detector center (x_D, y_D, z_D) in the fixed coordinate system can be expressed as

$$(x_F, y_F, z_F) = (R_0 \cos \lambda, R_0 \sin \lambda, 0) \quad (1)$$

$$(x_D, y_D, z_D) = (R_0 \cos \lambda, -H, 0) \quad (2)$$

Also, one can express the source trajectory $\mathbf{r}_s(\lambda)$ in the fixed coordinate system as

$$\mathbf{r}_s(\lambda) = (x_s, y_s, z_s) = (R_0 \cos \lambda, y_{s0}, 0) \quad (3)$$

where $y_{s0} = D \tan(\phi_1 + \phi_2) - H$, and

$$\phi_1 = \arctan \frac{H + R_0 \sin \lambda}{D} \quad (4)$$

$$\phi_2 = \arctan \frac{R}{\sqrt{D^2 + (H + R_0 \sin \lambda)^2 - R^2}} \quad (5)$$

As shown in Fig. 2, ϕ_1 is the angle between the x axis and the line connecting the FOV center and the detector edge, and ϕ_2 indicates the angle between the line connecting the FOV center and the detector edge and the line connecting the source and the detector edge.

Considering the physical constraint that the source cannot be within the object, we assume that the object support has a cylindrical shape, which has the same middle transverse slice as the ellipsoid object. Assuming that the long axis of the ellipsoid object is aligned with the x axis when $\lambda = 0$, we can rewrite the source trajectory in Eq. (3) as

$$\begin{aligned} \mathbf{r}_s(\lambda) = (x_s, y_s, z_s) = \\ (R_0 \cos \lambda, R_0 \sin \lambda + \max(y_{s0} - R_0 \sin \lambda, t), 0) \end{aligned} \quad (6)$$

where

$$t = \frac{-b^2 R_0 \sin \lambda + T(a, b, R_0; \lambda)}{a^2 \cos^2 \lambda + b^2 \sin^2 \lambda} \quad (7)$$

and

$$T(a, b, R_0; \lambda) = \sqrt{a^4 b^2 \cos^2 \lambda - a^2 b^2 R_0^2 \cos^2 \lambda + a^2 b^4 \sin^2 \lambda} \quad (8)$$

In general, reconstruction algorithms are developed for imaging configurations in which the object is fixed. Therefore, we need to determine the source trajectory in a coordinate system in which the object is fixed so

that these algorithms can be applied directly. In the case under study, we refer to the coordinate system fixed on the object as a object-fixed coordinate system (x_0, y_0, z_0) , which can be related to the original coordinate system (x, y, z) described above as

$$(x_0, y_0, z_0) = (x, y, z) \begin{bmatrix} \cos \lambda & -\sin \lambda & 0 \\ \sin \lambda & \cos \lambda & 0 \\ 0 & 0 & 1 \end{bmatrix} \quad (9)$$

Using x_s, y_s , and z_s to replace x, y , and z in the right-hand-side of Eq. (9), one can obtain the expression of the source trajectory $\mathbf{r}_0(\lambda) = (x_0, y_0, z_0)$ in the object-fixed coordinate system, which is displayed in Fig. 3.

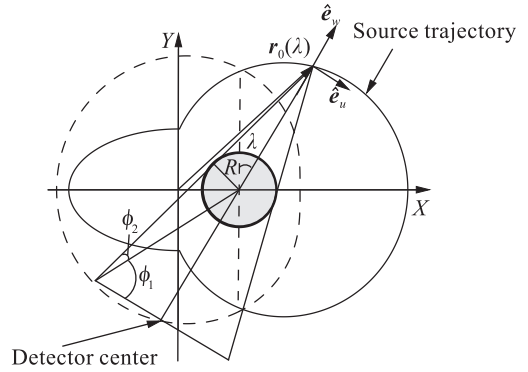


Fig. 3 Illustration of the scanning geometry in the object-fixed coordinate system. The thin solid and dashed lines represent the source trajectory and detector center trajectory respectively. The FOV is enclosed by the thick curve (shaded area).

2 BPF Algorithm for ROI-Image Reconstruction

2.1 Original BPF algorithm

In order to describe the original BPF algorithm, we introduce a rotation-coordinate system $\{u, v, w\}$, whose origin is fixed on the source point for the convenience of the reconstruction. Its three unit vectors in the fixed-coordinate system are

$$\begin{aligned} \hat{\mathbf{e}}_u &= (\cos \lambda, -\sin \lambda, 0)^T, \\ \hat{\mathbf{e}}_v &= (0, 0, 1)^T, \\ \hat{\mathbf{e}}_w &= (\sin \lambda, \cos \lambda, 0)^T \end{aligned} \quad (10)$$

Consider a flat-panel detector with its normal direction along $\hat{\mathbf{e}}_w$ and at a distance S from the source point. A 2-D coordinate system $\{u, v\}$ is assumed to be fixed on the detector plane and the u and v axes are

along the unit vectors \hat{e}_u and \hat{e}_v . Any point on the detector can thus be specified by two parameters u and v . At source position λ , the cone-beam projection of the object function $f(\mathbf{r})$ at a point (u_d, v_d) on the detector can be expressed as

$$P(u_d, v_d, \lambda) = \int_0^\infty f(\mathbf{r}_0(\lambda) + t\hat{\beta})dt \quad (11)$$

where

$$\hat{\beta} = \frac{1}{\sqrt{u_d^2 + v_d^2 + S^2}} [u_d \hat{e}_u(\lambda) + v_d \hat{e}_v(\lambda) - S \hat{e}_w(\lambda)] \quad (12)$$

is a unit vector indicating the direction of the ray that starts from source points $\mathbf{r}_0(\lambda)$ and passes through the point (u, v) on the detector.

The original BPF algorithm can reconstruct ROI images from truncated data acquired with a general trajectory by reconstructing images on chords. For a given continuous trajectory, a chord is a line segment connecting two points $\mathbf{r}_0(\lambda_a)$ and $\mathbf{r}_0(\lambda_b)$ on the trajectory. The form of the original BPF algorithm used here is given in Ref. [8], and the image on the chord specified by λ_a and λ_b is given by

$$f_c(x_c, \lambda_a, \lambda_b) = \frac{1}{2\pi^2} \frac{1}{b(x_c)} \cdot \left[\int_{x_{c1}}^{x_{c2}} \frac{b(x'_c) dx'_c}{x_c - x'_c} g_c(x'_c, \lambda_a, \lambda_b) + 2\pi P_0 \right],$$

where $b(x_c) = \sqrt{(x_{c2} - x_c)(x_c - x_{c1})}$ and P_0 denotes the projection data along the chord. $g_c(x_c, \lambda_a, \lambda_b)$ is defined by the following equation,

$$g_c(x_c, \lambda_a, \lambda_b) = \int_{\lambda_a}^{\lambda_b} \frac{d\lambda}{|\mathbf{r}(x_c) - \mathbf{r}_0(\lambda)|} \frac{d}{d\lambda} P(u_d, v_d, \lambda) \Big|_{\hat{\beta}} \quad (13)$$

By use of the original BPF algorithm, one can reconstruct ROI images from the truncated data acquired with the source trajectory described in Section 1. It can be observed that the weighting factor $\frac{1}{|\mathbf{r}(x_c) - \mathbf{r}_0(\lambda)|}$ in the back-projection step (i.e., Eq. (13)) is spatially varying, which can result in the increased noise level and computation load. We seek to eliminate such a factor by using the rebinned geometry, as discussed below.

2.2 Rebinned BPF algorithm

In the rebinned BPF algorithm, the acquired projection

data are first rebinned into the fan-parallel-beam geometry^[17-20]. The rebinned data can be expressed as $Q'(u_d, v_d, \varphi)$ satisfying

$$Q'(u_d, v_d, \varphi) = P(u_d, v_d, \lambda) \quad (14)$$

given that

$$\varphi = \lambda - \arctan \frac{u_d}{S} \quad (15)$$

By using this relationship, the weighting factor $\frac{1}{|\mathbf{r}(x_c) - \mathbf{r}_0(\lambda)|}$ in Eq. (13) can be eliminated.

3 Numerical Studies

We have performed computer-simulation studies to investigate and evaluate the rebinned BPF algorithm for achieving an ROI reconstruction for the trajectory described in Section 2. The numerical phantom is modified from a standard Shepp-Logan phantom. The center of the standard Shepp-Logan phantom is first shifted to the center of the FOV and the size of the Shepp-Logan phantom is then scaled to fit the size of the FOV. A long narrow ellipsoid object is placed at the rotation center which connects the Shepp-Logan phantom to the rotation axis. To cover the ROI, the FOV has a radius $R = 30$ cm and is at a distance $R_0 = 50$ cm from the physical center of rotation, and the detector has a size of $D = 64$ cm and is placed at a distance from the x axis at $H = 100$ cm. The detector has 512×512 units. Using these parameters in the imaging configuration, we computed cone-beam projection data from the rotating object at 720 views from $-\frac{\pi}{5}$

to $\frac{6\pi}{5}$, from which, noisy data were generated by adding Gaussian noise with a standard deviation that is about 1.5% of the maximum projection value. From these noiseless and noisy data sets, we have reconstructed the ROI images. In Fig. 4, we displayed the images reconstructed from the noisy data by use of rebinned and original BPF algorithms.

We have also performed a study to investigate the noise properties of the rebinned BPF. In this study, a uniform cylinder phantom was used. From the uniform phantom, we generated 1000 sets of the data containing stationary Gaussian noise. Without loss of generality, we focus on reconstructing images on a set of chords specified by $\lambda_1 = \frac{\pi}{4}$ and $\lambda_2 = \left[\pi, \frac{5\pi}{4}\right]$. Using

the 1000 images on these chords reconstructed from the noisy data sets, we calculated the empirical image variances on the chords. For comparison, the empirical image variances are obtained from the reconstructed images by use of the original BPF algorithm. The image variances along the chord specified by $\lambda_1 = \frac{\pi}{4}$ and $\lambda_2 = \frac{6\pi}{5}$ are displayed in Fig. 5. It can be observed that the rebinned BPF algorithm generally yields images with lower and more spatially uniform variances than does the original BPF algorithm. This uniform noise property in images obtained by use of the rebinned BPF algorithm is a direct result of the elimination of the spatially varying weighting factor from the back-projection in the rebinned BPF algorithm.

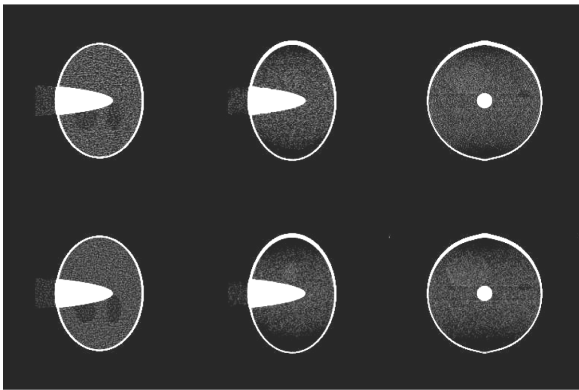


Fig. 4 The noisy images obtained with the rebinned BPF algorithm (top row) and the original BPF algorithm (bottom row) within the 2-D slices at $x=0$ mm, $y=0$ mm, and $z=0$ mm. The display window is [0.98, 1.2].

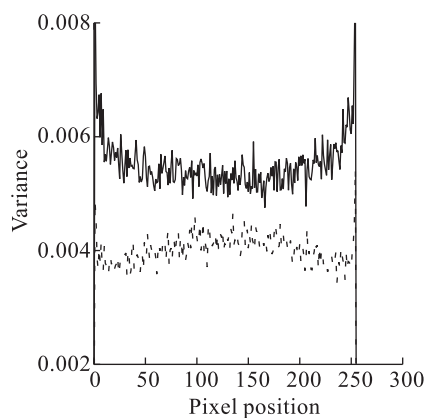


Fig. 5 Image variances on a chord, specified by $\lambda_1 = -\frac{\pi}{4}$ and $\lambda_2 = \frac{6\pi}{5}$, obtained by use of the rebinned BPF algorithm (dashed line) and original BPF algorithm (solid line)

4 Conclusions

In the work, we have described a rebinned BPF algorithm, which involves no spatially varying weighting factor in its back-projection step, for ROI-image reconstruction from truncated data acquired with a general trajectory. We have performed computation-simulation studies to validate and evaluate the rebinned BPF algorithm. The quantitative results demonstrate that the exact ROI-image reconstruction can be obtained with the rebinned BPF algorithm. Most important, the rebinned BPF algorithm can improve the noise properties in terms of image variances. It may find practical implications in numerous non-conventional CT scans involving general trajectories.

References

- [1] Katsevich A. Analysis of an exact inversion algorithm for spiral cone-beam CT. *Phys. Med. Biol.*, 2002, **47**: 2583-2597.
- [2] Zou Y, Pan X. Exact image reconstruction on PI-line from minimum data in helical cone-beam CT. *Phys. Med. Biol.*, 2004, **49**: 941-959.
- [3] Zou Y, Pan X. Image reconstruction on PI-lines by use of filtered backprojection in helical cone-beam CT. *Phys. Med. Biol.*, 2004, **49**: 2717-2731.
- [4] Zhuang T, Leng S, Nett B E, et al. Fan-beam and cone-beam image reconstruction via filtering the backprojection image of differentiated projection data. *Phys. Med. Biol.*, 2004, **49**: 5489-5503.
- [5] Pack J D, Noo F, Clackdoyle R. Cone-beam reconstruction using the backprojection of locally filtered projections. *IEEE Trans. Med. Imag.*, 2005, **24**: 2317-2336.
- [6] Pack J D, Noo F. Cone-beam reconstruction using 1D filtering along the projection of m-lines. *Inv. Prob.*, 2005, **21**: 1105-1120.
- [7] Yu H, Ye Y, Zhao S, et al. A backprojection-filtration algorithm for nonstandard spiral cone-beam ct with n-PI-window. *Phys. Med. Biol.*, 2005, **50**: 2099-2111.
- [8] Zou Y, Pan X, Sidky E Y. Theory and algorithms for image reconstruction on chords and within region of interests. *J. Opt. Soc. Am. A: Opt. Image Sci. Vis.*, 2005, **22**: 2372-2384.
- [9] Noo F, Clackdoyle R, Pack J. A two-step Hilbert transform method for 2D image reconstruction. *Phys. Med. Biol.*, 2004, **49**: 3903-3923.
- [10] Pan X, Zou Y, Xia D. Peripheral and central ROI-image

- reconstruction from and data-redundancy exploitation in truncated fan-beam data. *Med. Phys.*, 2005, **32**: 673-684.
- [11] Defrise M, Noo F, Clackdoyle R, et al. Truncated Hilbert transform and image reconstruction from limited tomographic data. *Inv. Prob.*, 2006, **22**: 1037-1053.
- [12] Bian J, Zhang H, Zhang P, et al. A cone-beam approach of ROI imaging with a detector smaller than the imaged object. In: *Proceedings of the 2007 International Meeting on Fully 3D Image Reconstruction in Radiology and Nuclear Medicine*. Lindau, Germany, 2007: 386-389.
- [13] Besson G. CT image reconstruction from fan-parallel data. *Med. Phys.*, 1999, **26**: 415-426.
- [14] Pan X. Optimal noise control in and fast reconstruction of fan-beam computed tomography image. *Med. Phys.*, 1999, **26**: 689-697.
- [15] Xia D, Yu L, Sidky E Y, et al. Noise properties of chord-image reconstruction. *IEEE Trans. Med. Imaging*, 2007, **26**: 1328-1344.
- [16] Dennerlein F, Noo F, Hornegger J, et al. Fan-beam filtered backprojection reconstruction without backprojection weight. *Phys. Med. Biol.*, 2007, **52**: 3227-3240.
- [17] Grass M, Köhler T, Proksa R. 3D cone-beam CT reconstruction for circular trajectories. *Phys. Med. Biol.*, 2000, **45**: 329-347.
- [18] Turbell H. Cone-beam reconstruction using filtered back-projection [Dissertation]. Linköping University, Linköping, Sweden, 2001.
- [19] Heuscher D, Brown K, Noo F. Redundant data and exact helical cone-beam reconstruction. *Phys. Med. Biol.*, 2004, **49**: 2219-2238.
- [20] Yu L, Xia D, Zou Y, et al. A rebinned backprojection-filtration algorithm for image reconstruction in helical conebeam CT. *Phys. Med. Biol.*, 2007, **52**: 5497-5508.

Image Reconstruction for Breast CT Using Sparse Projections

Junguo Bian, Xiao Han, Kai Yang*, Nathan Packard*, Emil Y. Sidky, John M. Boone* and Xiaochuan Pan

Department of Radiology, The University of Chicago

5841 S Maryland Avenue, Chicago, IL 60637

*University of California Davis Medical Center

4860 Y Street, Sacramento, CA 95817

I INTRODUCTION

Breast cancer is the most frequently diagnosed cancer and the second leading causes of cancer mortality among woman. Researchers are actively developing x-ray breast imaging techniques that can form three-dimensional image of the breast, including breast tomosynthesis and dedicated breast computer tomography CT. Several prototype dedicated breast CT scanners have been built in different institutions throughout US. Most of the scanners have a circular configuration and adopted an approximate analytic reconstruction algorithm, which requires a large number of views to be acquired. The total dose of a breast CT scan is normally about the same as a two-view mammogram. It is still desirable to further reduce the breast CT dose for general screening purpose.

Inspired by the principle of compressive sensing, we have proposed algorithms for image reconstruction from fan- and cone-beam data collected at highly sparse views through minimization of the total variation (TV) of the image subject to the condition that the estimated data is consistent to the measured data. The advantage of our TV minimization algorithm is that by reducing the number of views, total dose can be reduced significantly. In this study, we investigate the sparse data reconstruction for breast CT by using very few projections. The aim of this study is to perform a preliminary investigation to further reduce the dose of breast CT for breast cancer screening.

II MATERIALS AND METHODS

The breast CT data were acquired by a clinical trial conducted by our collaborator at UC-Davis medical center. The prototype scanner consists of a water-cooled tungsten anode x-ray tube, a flat-panel CsI indirect x-ray detector that was 40 cm wide and 30 cm tall and an integrated bearing-motor-encoder system. The detector has a pixel matrix of 1024×768 , with pixel size of 0.388 mm. The source to detector distance is 87.78 cm and the source to rotation center is 45.83 cm. For each data sets, 500 cone-beam pro-

jection images are acquired 360° around the patient's breast in 16.6 seconds.

In the TV algorithm, the imaging system is modeled by a discrete linear system $\vec{g} = M\vec{f}$, where \vec{g} is the measured, \vec{f} denotes the discrete image and M is the system matrix. The TV algorithm is formulated into a constrained TV-minimization framework, which seeks to find image \vec{f} that minimizes its TV: $\vec{f}^* = \text{argmin} \|\vec{f}\|_{TV}$, subject to the data fidelity and non-negativity constraints. The proposed TV algorithm solves this constrained optimization problem through using a hybrid scheme in which the projection onto convex sets (POCS) is used to enforce the data constraint, and gradient descent method is used subsequently for minimizing the image TV.

In order to investigate the performance of the TV algorithm, we extract the mid-slice sinogram from the patient data and add simulated sinogram. The simulated sinogram is generated by analytic phantom with exactly the same geometry as the prototype breast CT scanner. The analytic phantom consists of small ellipsis to mimic small structures in the breast with their sizes varying from 0.5 mm to 1.3 mm. The intensity of the structures are about 0.5 to 1. times of the intensity of the background glandular tissues. The modified patient breast image is shown in the first column of Figs 1 to 4 and the white dots show the small structures, the intensity of the small structures are about 1.5 to 2 times of the background tissues.

In order to study the effects of the noise, we also average mid-slice sinogram with its two neighboring detector rows to form the new mid-slice sinogram and add simulated sinogram to this new sinogram. By averaging, the noise level in the projection data is effectively reduced. From the full 500 views of projection data sets of the mid-slice sinogram with and without averaging, we extract 25 and 50 views of projection data which are uniformly distributed from 0 to 360° . We used both TV and FDK algorithms to reconstruct images from these four sparse data sets. The reconstruction image size is $15 \times 15 \text{ cm}^2$ and the corresponding image array size is 512×512 .

Because the total dose of breast CT need to be distributed over a large number of views (usually several hundred), there are considerable quantum noise in the images reconstructed directly by FDK algorithms. So we applied a hanning filter to the images reconstructed by FDK algorithms. For TV, we take the images at the 40th iteration.

III RESULTS

In Figs. 1 to 4, we displayed the images reconstructed by use of TV and FDK for the mid-slice sinogram and the averaged sinogram. In Fig 1., the 25-view FDK reconstruction is clearly overwhelmed by the streaks caused by aliasing and it is very difficult to differentiate between real structures and artifacts. However, the image reconstructed by TV algorithm is free of streak artifacts and some of the structures can be easily identified. In Fig 2., we displayed the TV and FDK reconstruction from the 25-view averaged sinogram. Both the FDK reconstruction and TV reconstruction become better in this case. However, the FDK image is still dominated by the streak artifacts, while almost all four groups of the small structures can be identified in the TV reconstruction image. In Fig 3, we displayed the TV and FDK reconstruction from the 50-views of projection data without averaging. There are still artifacts caused by aliasing and the artifacts have very close appearance to the small structures, which will caused many false positives. While in the TV reconstruction images, the structures can be visualized much better and all the structures can be identified in the image. In Fig. 4, we displayed the TV and FDK reconstruction from the 50-views averaged sinogram. The visualization of the structures are almost the same in this case.

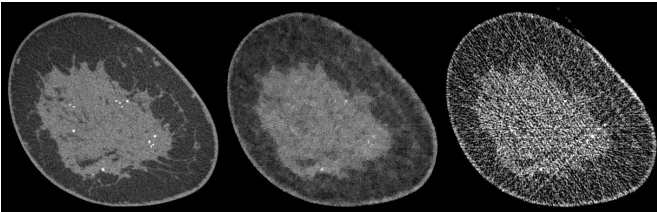


Fig. 1. Image reconstructed by TV (middle) and FDK (right) algorithms using 25 views of projection data without averaging. The modified breast image (left) shows the small structures. The display window is $[0.15, 0.28] \text{ cm}^{-1}$.

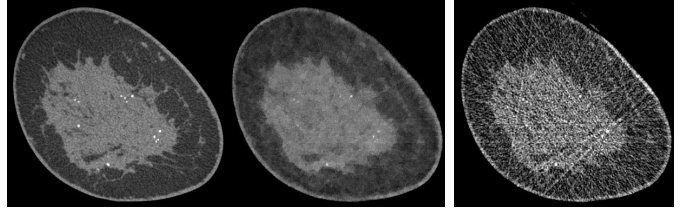


Fig. 2. Image reconstructed by TV (middle) and FDK (right) algorithms using 25 views of projection data from the averaged sinogram. The modified breast image (left) shows the small structures. The display window is $[0.15, 0.28] \text{ cm}^{-1}$.

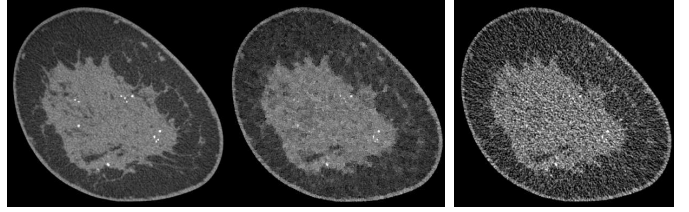


Fig. 3. Image reconstructed by TV (middle) and FDK (right) algorithms using 50 views of projection data without averaging. The modified breast image (left) shows the small structures. The display window is $[0.15, 0.28] \text{ cm}^{-1}$.

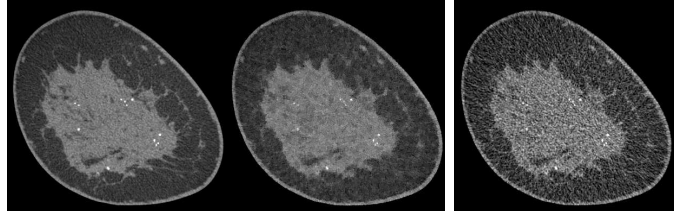


Fig. 4. Image reconstructed by TV (middle) and FDK (right) algorithms using 50 views of projection data from the averaged sinogram. The modified breast image (left) shows the additional small structures. The display window is $[0.15, 0.28] \text{ cm}^{-1}$.

IV DISCUSSION

A preliminary study of sparse data reconstruction for breast CT using TV minimization algorithm is performed by using real patient data with adding small structures added to the breast. By comparing the FDK reconstruction and TV reconstruction, it can be seen that the structures can be visualized much better in image reconstructed by TV algorithm than the images reconstructed by FDK for 25 views of projection data of the two different noise levels since the streak artifacts dominated the FDK reconstruction. For images reconstructed from 50views of projection data, the streak artifacts are not a serious issue any more. However, the TV reconstruction is still better in visualization of the small structures for the sinogram without averaging while the visualization is about the same for images reconstructed by TV and FDK from the 50-view averaged sinogram. This study demonstrate that the breast CT dose can potentially be reduced to a very low level for screening purpose by use of very sparse projection data.